Hindawi Publishing Corporation
Journal of Nanotechnology
Volume 2010, Article ID 487193, 12 pages
doi:10.1155/2010/487193

Review Article

Epitaxial Growth of Ru and Pt on Pt(111) and Ru(0001), Respectively: A Combined AES and RHEED Study

M. S. Zei

Department of Physics, National Central University, No. 300 Jungda Road, Jungli 32054, Taiwan

Correspondence should be addressed to M. S. Zei, zei@phy.ncu.edu.tw

Received 30 October 2009; Revised 10 February 2010; Accepted 27 February 2010

Academic Editor: Charles M. Lukehart

The epitaxial growth of Pt and Ru deposits by spontaneous, as well as by dynamic, electrodeposition onto Ru(0001) and Pt(111), respectively, have been studied by reflection high energy electron diffraction (RHEED) and Auger electron spectroscopy (AES). For the Pt deposit on Ru(0001), at submonolayer range, it preferably grows compressed commensurate bilayer thick islands on Ru(0001). This is the first time that RHEED observation of the onset of Pt twinning occurs in ca. 2-3 layer thick islands on Ru at room temperature, at which the surface strain due to the 2.5% lattice mismatch of Pt and Ru remains intact. For multilayer thick islands (>6 ML) ordered reflection twins (diameter of ~3 nm) develop and are embedded in a (111) matrix with an incoherent (11-2) twin plane normal to Ru(0001) and aligned with their [−110] direction parallel to the [11-20] Ru(0001) substrate direction. For the Ru deposit on Pt(111), at ~0.2 ML a strained (1×1) monoatomic layer is formed due to the 2.5% lattice mismatch of Ru and Pt. Increasing the coverage up to ~0.64, the second Ru layer is found to relieve the strain in the first layer, giving rise to dislocations and Ru relaxes to its bulk lattice constant. Multilayers of Ru (>1 ML) result in (0001) nanocluster formation aligned with its [11-20] direction parallel to the [−110] Pt(111) substrate direction.

1. Introduction

Considerable attention has been given to the growth of mixed metals, which enables the preparation of materials with particular chemical properties. Apart from evaporation in UHV [1, 2], also spontaneous [3–5] or electrochemical deposition [6–8] from electrolyte solution has been used most often to prepare the modified catalyst surfaces. This interest stems from the possibility of preparing modified electrodes as model systems to probe the reactivity at the interfaces. The most widespread and promising bimetal-catalysts for fuel cell (FC) applications employ dispersed bimetal nanoparticles as electrocatalysts, usually a platinum based alloy. Bimetallic Pt catalysts, mainly Pt-Ru [9–11], but also Pt-Sn [12], Pt-Mo [13], and Pt-Os [14], have been intensively studied in order to achieve the optimal electrooxidation of methanol via the so-called bifunctional mechanism [15, 16]. Spontaneous deposition has been used to prepare the Ru-modified Pt(111) [7, 17] as well as Pt/Ru(0001) surfaces [4, 18, 19]. Remarkable enhancements of the electrocatalytic activity towards CO, methanol, and formic acid oxidation have been found with both Ru-modified Pt electrode and Pt-modified Ru electrodes [4, 18, 19]. The spontaneously deposited Ru on Pt(hkl) surface showed considerable catalytic activity for methanol oxidation [19, 20], where the Ru deposit was reported to be not higher than 20% coverage, as inferred from AES and STM measurements. Moreover, it was found that the compressed Pt adlayer on Ru(10-10) leads to enhanced catalytic activity towards CO oxidation [16]. In order to understand the mechanism of CO/methanol electrooxidation on bimetal catalysts, more work on the surface structure and the relationship between the surface structure and the reactivity of catalysts is necessary. Therefore the nanostructure of bimetal surfaces has been extensively studied; previous studies, using scanning probe methods, reported the spontaneous deposition of Pt resulting in 3–10 nm sized Pt clusters grown on Ru(0001) [5]. Similar conclusions were obtained from AES and RHEED investigations of Pt spontaneous deposition onto Ru(0001) [4]. On the other hand, several deposition

studies for Pt on Ru(0001) in UHV have been reported; evaporating platinum onto a clean Ru(0001) surface leads to the formation of monolayer islands with a characteristic, dendritic shape, that are homogeneously distributed over the terraces for 0.4 ML Pt deposited on Ru(0001) in UHV [21]. Schlapka et al. [22, 23] have found smooth Pt adlayer up to 4 ML and the dislocation lines at 8 ML thick film for Pt deposited on Ru(0001) by electron bombardment of a Pt rod, where the temperature range of Pt deposition and annealing was kept below 800 K to avoid intermixing at the Pt-Ru interface [21]. Recent work, using X-ray photoelectron spectroscopy (XPS), reported that the Pt(II) oxidation state rather than the metallic state of Pt deposit is observed after Pt spontaneous deposition (< 0.3 ML) on Ru(0001) [24]. For Ru deposited on Pt(111) by spontaneous deposition in situ scanning tunneling microscopy (STM) studies have demonstrated that the formation of monolayer and bilayer thick islands is coverage dependent; at 0.18 ML it results in a predominantly monolayer thick island (∼76%), while at 0.3, bilayer and multilayer thick islands develop [20, 25, 26]. Vapor deposition of about 1 ML ruthenium onto a clean Pt(111) surface and subsequent short annealing to 820 K leads to the formation of 3D-islands having a width of 5–10 nm [27]. Furthermore, the lattice strain of an admetal layer with the underlying substrate may result from their lattice mismatch, like that found for Pt on Ru(10-10) [16], Co on Pt(111) [28], Ag on Pt(111) [29], and Cu on Ru(0001) [30]; it is expected to gradually vanish for two, three, or more layers, leading to lattice dislocations as observed for Pt overlayer on Ru(0001) [4, 23] and Ru on Pt(111) observed in the present work. It is a pity that the formation of the twinned Pt nanoclusters on Ru(0001) has not been mentioned and discussed by the reported works [5, 21–24]. In this paper, we have provided complements to the previous works [4, 7] and focused the interest on the initial stages of Pt twin formation and its epitaxial growth on Ru(0001). Also the layer dependence of the lattice strain of Pt and Ru on Ru(0001) and Pt(111), respectively, will be addressed. We report here for the first time RHEED data showing that the onset of Pt twinning occurs in ∼2-3 layer thick islands on Ru(0001), in which the lattice strain within the twinned Pt particles still remains. On the other hand, for Ru deposited on Pt(111), at ∼0.2 ML coverage, strained (1×1) commensurate monolayer islands are mainly formed on Pt(111), while at coverage 0.64 the second Ru layer is found to relieve the strain in the first layer, giving rise to a dislocation. There is no twinning for various Ru coverages on Pt(111). Furthermore our results will be compared with those recently published works dealing with the Ru and Pt deposition on Pt(111) and Ru(0001), respectively.

2. Experiment

The experiments were performed with an apparatus consisting of a UHV chamber (base pressure $< 2 \times 10^{-10}$ mbar) incorporating LEED, RHEED, and AES, an electrochemical chamber (base pressure $< 2 \times 10^{-9}$ mbar), an electrochemical cell, and a closed sample transfer. The detailed surface analysis and electrochemical experiments have been reported elsewhere [31, 32]. The working electrode, an Ru(0001) or a Pt(111) single crystal disc of 7 mm diameter and 2 mm thickness, was mounted between tungsten wires which also served for resistive heating of the sample. The Pt and Ru electrode surfaces were prepared by cycles of argon ion bombardment and annealing (∼1300 K), until the sample surface was free from disorder and impurities, as controlled by RHEED and AES [32]. The Pt deposition onto Ru(0001) was first performed by spontaneous deposition by immersion of the electrode into a 0.1 M $HClO_4$ solution containing 0.1 mM H_2PtCl_6 without the application of an external potential. Deposition of Ru was carried out with freshly prepared solutions of 0.01 to 5 mM $RuCl_3$ in 0.1 M $HClO_4$. After Pt/Ru deposition the emersed Ru/Pt electrodes were rinsed thoroughly with 0.1 M $HClO_4$ solution and then Millipore water. The sample was then pumped down under vacuum and transferred to the main chamber for AES and RHEED analysis. A platinum wire with 0.4 mm diameter was used as the counter electrode in the electrolyte vessel on top of a glass capillary [31]. The Ru coverage was determined by AES from the intensity ratio $I_{Ru,200}/I_{Pt,257}$ and the increased charge in the double-layer region of the cyclic voltammogram (between 0.35 V and 0.6 V versus RHE) [7, 33]. After several deposition experiments, the deposit on the sample surfaces was removed by stripping in Pt- and Ru-free acid solutions and subsequently cleaned by repeated sputtering/annealing cycles in UHV. When the cleaning processes were no longer able to remove the residues of Pt/Ru from the Ru(0001)/Pt(111) surfaces, the sample was removed from the UHV system and polished with 0.02 μm alumina followed by careful rinsing with Millipore water. In order to check the cleanliness of the Ru/Pt electrodes and the electrolyte vessel, the cyclic voltammogram for the clean Pt(111)/Ru(0001) electrodes was first recorded in a 0.1 M $HClO_4$ solution prior to Ru/Pt deposition [4, 7].

3. Results

3.1. Spontaneous and Electrodeposition of Pt on Ru(0001). Prior to Pt electrodeposition the cleaned Ru(0001) surface was first probed by AES and RHEED. RHEED patterns (Figures 1(a) and 1(b)) for a clean Ru(0001) surface reveal a (1×1) structure, showing a well-ordered Ru substrate surface. The cleanliness of the Ru electrode was controlled by Auger electron spectroscopy (AES) as shown in Figure 2(a), whereby the impurities were absent, since the detected Auger intensity ratio of I_{273}/I_{231} is about 2.1 (refer to Figure 2(a)) which is lower than that of a clean Ru surface ($I_{273}/I_{231} \sim 2.5$) [34]. If the carbon impurities were present in the Ru sample, the value of I_{273}/I_{231} will be significantly increased, and the background intensity will remarkably increase in LEED/RHEED. In contrast, both LEED (not shown) and RHEED patterns show sharp reflections with high contrast; it is reasonable to conclude that the Ru sample is clean. Moreover, a clean and well-ordered Ru sample annealed at 1300 K has also been controlled by the cyclic current-potential curves in 0.1 M $HClO_4$ where two

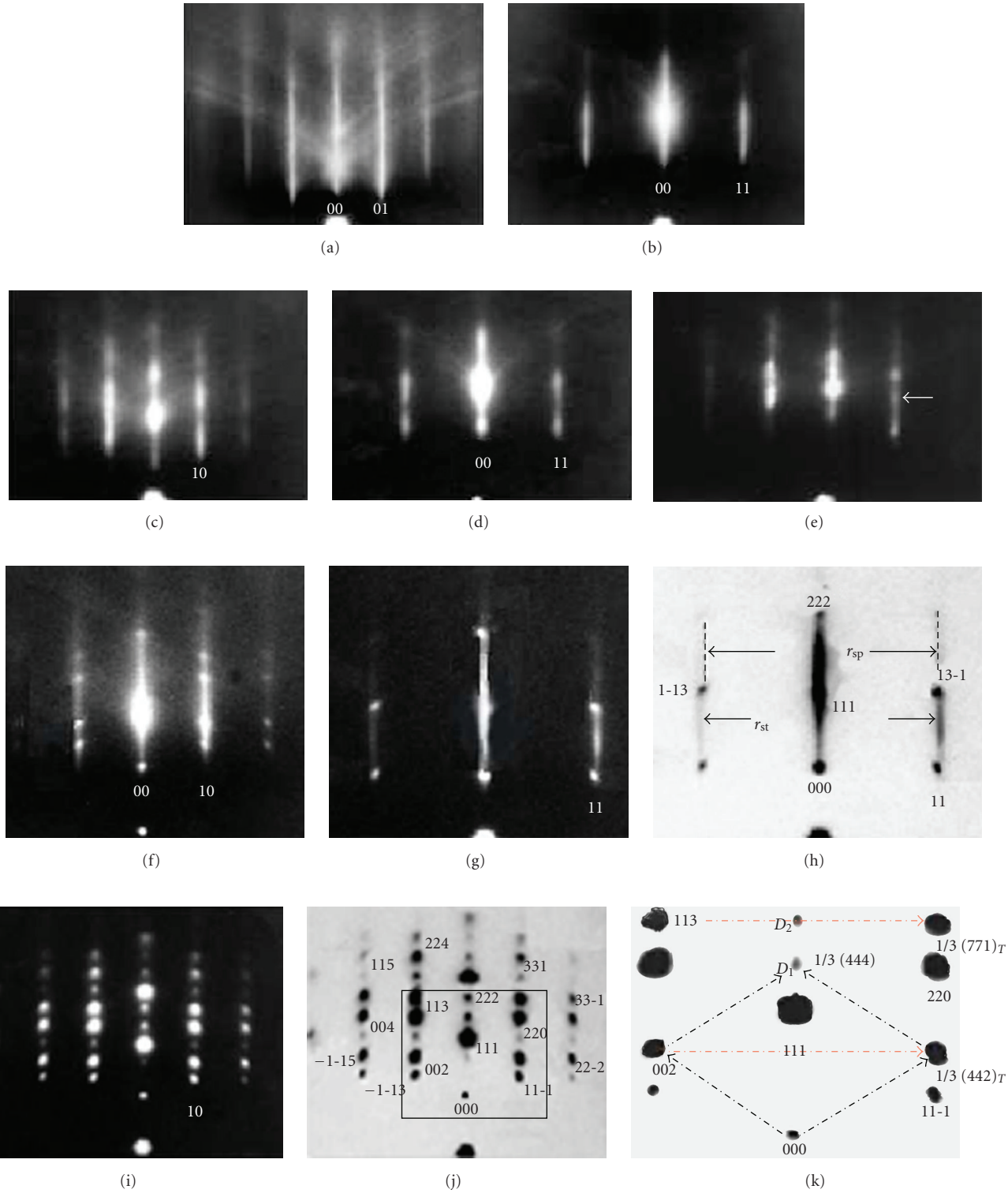

Figure 1: (1 × 1) RHEED patterns ([11-20] (a) and [0110] (b)) for Ru(0001) after argon ion sputtering and annealing at 1300 K under UHV conditions, showing 2D reflection streaks of the (±10) and (±11) beams; the RHEED patterns ([11-20] (c) and [0110] (d)) for Ru(0001) electrode covered by submonolayer Pt, showing intensity modulation along the substrate reflection rods; the RHEED pattern ([11-20]) for the Ru(0001) electrode covered by Pt deposit after second spontaneous deposition, showing additional reflection depicted by the arrow along the Ru substrate reflections (±10); the RHEED patterns ([11-20] (f) and [0110] (g)) for the Ru(0001) electrode covered by Pt (>1 ML) by spontaneous deposition (>3 min), showing 3D spots due to the Pt clusters; the indexed reciprocal lattice (h) of Figure 1(g); the RHEED pattern [11-20] (i) and its indexed reciprocal lattice (j) for the Ru(0001) electrode covered by Pt (>1 ML) by electrodeposition; (k) the indexed reciprocal lattices of the matrix and the twin for the marked part of Figure 1(j).

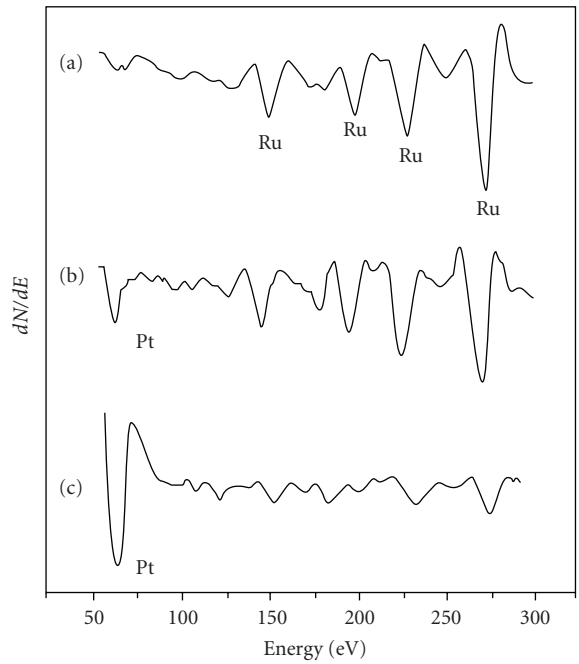

Figure 2: Auger electron spectra: (a) for a clean Ru(0001) surface after argon ion sputtering and annealing under UHV conditions, (b) for an Ru(0001) electrode covered with a submonolayer Pt by spontaneous deposition, and (c) the Ru electrode with Pt clusters formed by electrodeposition.

voltammetric peaks develop at −0.15 and 0.25 V versus Ag/AgCl, indicative of a clean Ru surface [35]. The structural analysis of the Pt/Ru-deposits on Ru(0001) and Pt(111) has been predominantly performed by RHEED. The observed RHEED pattern actually corresponds to a reciprocal lattice plane (uvw)*, which is a cross-section of a reciprocal lattice (rel) sliced by a reflection sphere (Ewald sphere) at the [uvw] zone axis. It is a (uvw)*-plane of (hkl)-rel points (relps) of zero-level with respect to the [uvw] zone axis illustrated by Figure 3(a), where the (hkl) planes are parallel to the [uvw] zone axis satisfying the zone condition, hu + kv + lw = 0. The inset in Figure 3(a) shows a (−110)* rel plane of an fcc crystal with respect to the [−110] zone axis. Based on the rel planes obtained at two azimuths one can construct a rel of a nanocluster and determine the phase and the orientations of the Pt and Ru clusters grown on the substrate surfaces. First the sample was prepared by spontaneous deposition through short immersion (<1 min) into the Pt^{4+} containing $HClO_4$ solution. A pronounced Auger Pt-signal develops at 65 eV for the Pt covered Ru(0001) surface (Figure 2(b)) compared with that of a clean Ru(0001) surface in Figure 2(a), indicating the presence of a Pt deposit on Ru(0001). The RHEED patterns from a Pt-covered Ru(0001) surface also show a (1 × 1) structure (Figures 1(c) and 1(d)); however, the (±10) and (±11) substrate reflection streaks show intensity modulation (compare with Figures 1(a) and 1(b)). From the intensity profile analysis of the streaked reflections it was found that the Pt bilayer thick islands grew predominantly on Ru(0001), and some population of mono- and multilayer islands may also be present. The intensity profile was calculated with an interference function $\sim\sin^2(\pi NL)/\sin^2(\pi L)$, where L is an integer and N is the number of adlayers (refer to [7]). The lateral spacing of the Pt-bilayer matches with the Ru substrate, since the 2D-rods of the Pt layers coincide with those of the substrate (±10) rods (Figure 1(c)); that is, both LEED (not shown) and RHEED patterns show no extra reflections, indicating that the Pt adlayer is commensurated (1 × 1) with the Ru(0001) substrate surface, where the mean domain size of Pt islands is about 3-4 nm estimated from the width of the Pt reflection streak in RHEED. The average diameter (D) of the islands (nanoclusters) is estimated by the formula $w/a^* = a/D$ [36, 37] where w and a^* are the mean spot diameter and the reflection rod spacing in the RHEED pattern at the [uvw] azimuth, respectively, and a is the [uvw] atomic row spacing. It implies that the Pt [−110] atomic row spacing is compressed by 2.5% with respect to the bulk Pt in order to match with the [11-20] row spacing of the Ru substrate in good agreement with the results obtained by Schlapka et al. probed by CO adsorption on the strained Pt layer on Ru(0001) [22, 23]. For that the morphology of the Pt (1–4 ML) film on Ru(0001) is prepared by electron bombardment of a Pt rod under UHV conditions, and subsequent annealing below 800 K was very smooth [22]. On the other hand, monolayer Pt islands with dendritic shape were observed for Pt deposition of about 0.4 ML on Ru(0001) at room temperature in UHV, and subsequent annealing at 800 K causes these islands to collapse and induces a ripening process, forming the 2–13 nm sized Pt clusters dispersed on Ru(0001) [21]. The size distribution of Pt clusters and the growth behavior of the Pt islands on Ru(0001) prepared in UHV differ clearly from those of the electrodeposition, since the Pt deposit is coadsorbed by the anions during the electrodeposition [38, 39]. It should be noted that the shape and the island distribution could not be obtained by RHEED, but the in-plane lattice constant of Pt islands could be precisely determined from the diffraction patterns. After the second spontaneous deposition, the Pt- and Ru-rods (±10) still overlap in the RHEED pattern (see Figure 1(e)), indicating that the Pt lattice strain still remains; that is, the Pt adlayer is still commensurated (1 × 1) with the Ru(0001) substrate surface. Note that the additional diffused spot depicted by the arrow develops between the Pt (220) and (11-1) matrix spots along the (10)-substrate reflection rod (refer to Figure 1(e)), the extra spots could not be assigned straightforwardly from Figure 1(e), since their locations are not resolvable with respect to the Pt matrix spots, and it will become evident latter that they are due to twinning derived from a well-defined diffraction pattern of Figures 1(f) and 1(i) (see Section 4). We consider the diffraction pattern from a deposit-film containing a fault in terms of two reciprocal lattices: one "normal" pattern corresponding to the matrix, and the other consisting of the twins, superimposed. Since the fault plane is one of the four (111) in fcc, and because the unique crystallographic relations exist between the fcc (Pt) and hcp (Ru) lattices, the rel-rods will lie along ⟨0001⟩ hcp parallel to ⟨111⟩ fcc throughout the reciprocal lattice. A longer immersion time

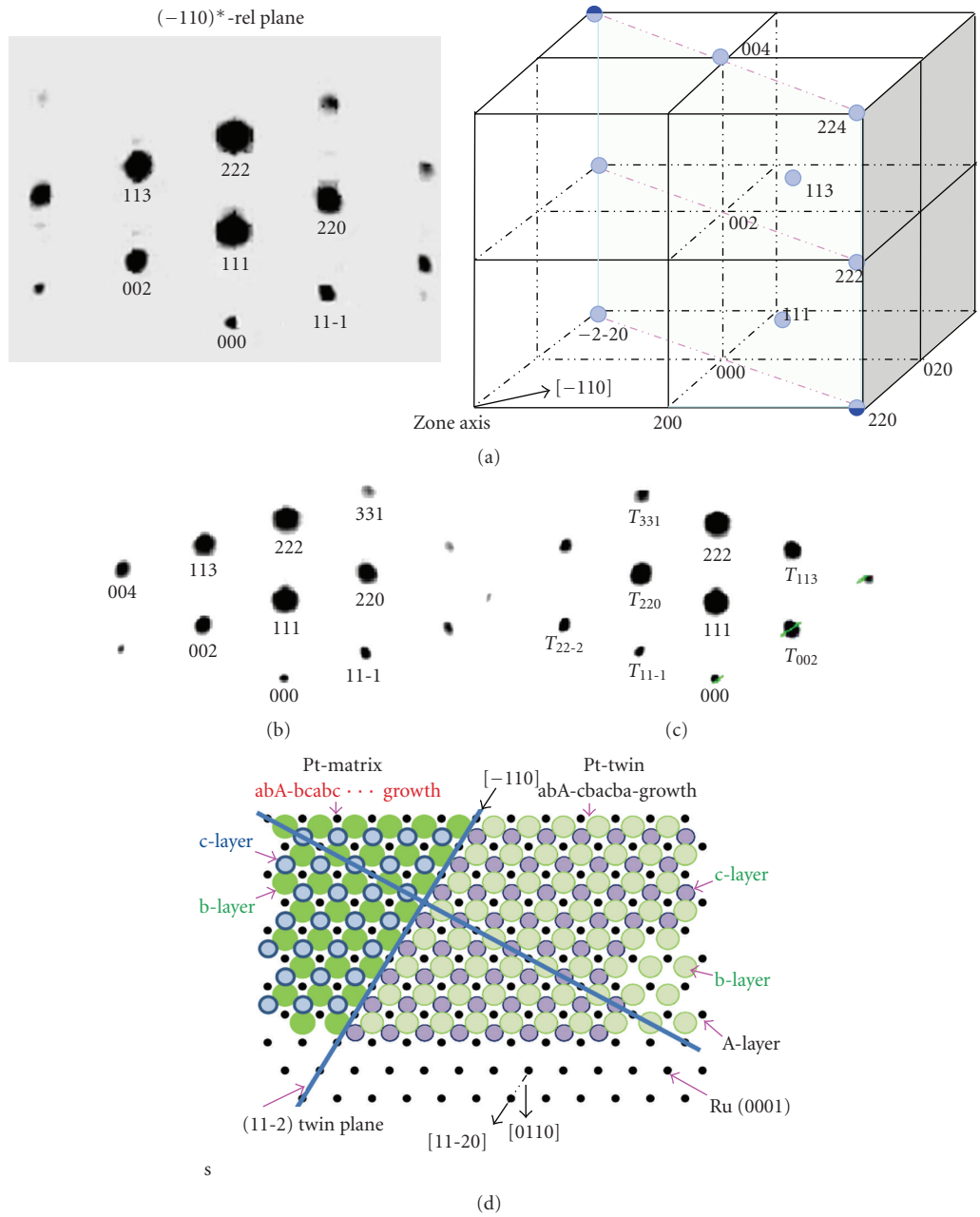

FIGURE 3: A reciprocal lattice intersected by a reflection sphere giving rise to a rel plane as shown by the inset (a); a (−110)* rel-plane of the Pt matrix (b) and the corresponding (−110)* plane of the twin crystal (c); schematic diagram of an ordered Pt matrix (crystal I) besides the twin (crystal II) grown on Ru(0001), where the [−110] deposit direction is parallel to the [11-20] Ru(0001) substrate direction.

~3 minutes results in cluster formation, demonstrated by 3D-reflection spots superimposed on the streaky substrate reflections in Figures 1(f) and 1(g), where pronounced extra spots clearly develop besides the Pt matrix spots. From the width of the spots an average cluster size of ~3 nm (with thickness of about 10 ML) is determined close to that estimated by the STM study [5]. The streaked substrate reflection characterizes a flat substrate surface so that the Ru(0001) surface is not completely covered by the Pt deposit, for that the Pt clusters cover about 30% of the Ru surface detected by SEM (not shown) [4] close to the STM results [5, 10]. With island thickness of ~10 ML, Pt relaxes and continues growing with its own lattice parameters confirmed by the inset in Figure 1(h), where the spot-spacing of the Pt cluster depicted by r_{sp} is ~2.5% smaller than the reflection rod-spacing (r_{st}) of the Ru substrate, in which r_{sp} and r_{st} are the double spacing of the Pt (02-2)-reflection and Ru (1-20)-reflection, respectively. This demonstrates that Pt relaxes to its bulk lattice constant supported also by the estimated spot spacing of 0.443 A^{-1} along the (00)-beam, which is the reciprocal value of the (111) lattice spacing of bulk Pt (1/2.26 A). These findings exhibit some analogy

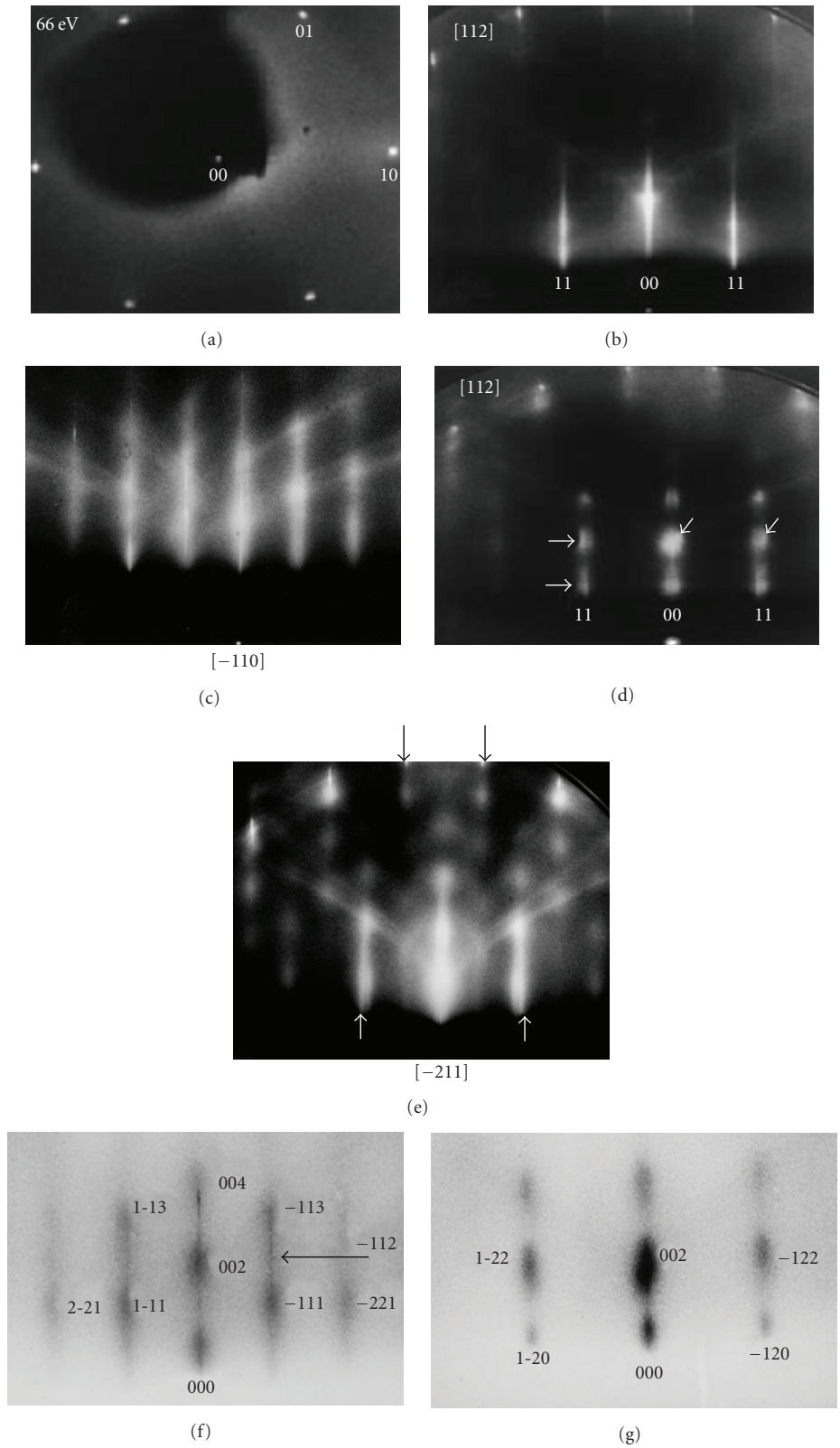

Figure 4: (a) LEED (66 eV) and (b) the RHEED ([112] azimuth) patterns for an Ru-deposited Pt(111) electrode surface (0.25 ML); the RHEED patterns (c) ([110]) and (d) ([112]) for an Ru-deposit modified Pt(111) electrode surface with the Ru coverage of 0.64, showing intensity modulation and satellite reflections besides the Pt substrate reflections; (e) the RHEED pattern ([−211]) obtained at another position of the electrode surface, where both the Pt- and satellite-reflections are clearly resolvable at the first- and zero-Laue zones; the RHEED patterns (f) ([−110]) and (g) ([−211]) for an Ru-modified Pt(111) electrode surface with ∼1 ML coverage.

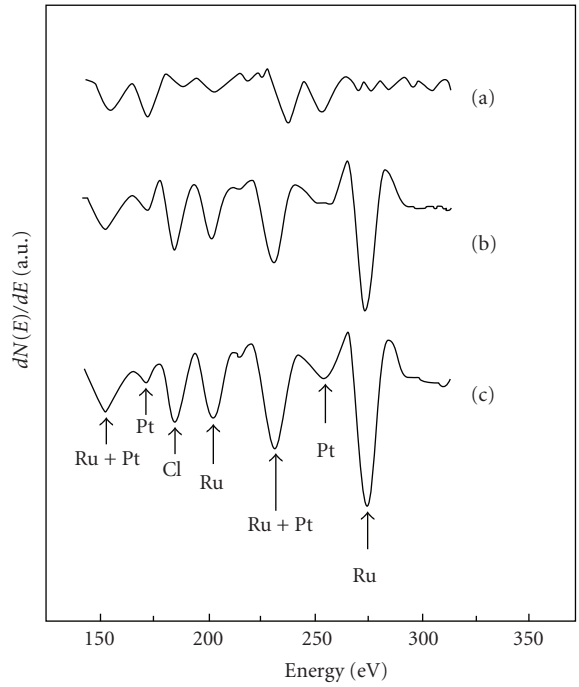

FIGURE 5: Auger electron spectra of the pure Pt(111) (a) and Ru-modified Pt(111) electrodes with 0.64 (b) and ~1 ML Ru coverage (c).

to those observed for Pd electrodepositon onto Au(100) at higher coverage (>6 ML) [6]. This shows that the Pt coverage and cluster formation are related to the time of the Ru crystal immersion. In order to study the dependence of the epitaxial growth upon the coverage and the deposition process, the Pt deposition was done by 10 cycles of potential sweeping between −0.2 to +0.3 V versus Ag/AgCl. The RHEED patterns for the Pt-electrodeposited Ru(0001) electrode show only 3D-reflection-spots in Figures 1(i) and 1(j), whereby the Ru electrode was completely covered by 2–8 nm-sized Pt-clusters confirmed by SEM [4] and STM [5] images (not shown). As expected, its AES spectrum shows a dominated Auger Pt-signal in Figure 2(c), while the Ru-signal is strongly suppressed. At the $[0110]_{Ru}$ azimuth, parallel to the [−211] direction of the Pt clusters, the spacing between the spots at the (00)- and (11)-beams parallel to the substrate surface is $0.72\,A^{-1}$ (see Figure 1(g)) equal to the 02-2 reflection of the fcc Pt crystallites ($0.7209\,A^{-1}$). This demonstrates that Pt dynamically electrodeposited on Ru(0001) relaxes to its bulk lattice constant at ~5–10 ML thick islands, in agreement with the former results obtained from longer immersion (≅3 min). The rel plane $(-211)^*$ including the 02-2 and 000 points lies in the zero-level with respect to the $[-211]_{Pt}$ zone axis. Thus a bcc-reciprocal lattice (body-centered cubic (bcc)) is derived from the rel-planes obtained at two azimuths; that is, in real space the fcc Pt nanloparticles are growing with (111) plane on Ru(0001). Closer inspection of Figures 1(f) and 1(i) reveals that besides the relps of the Pt matrix additional spots appear at [11-20] azimuth in the RHEED, in which the $(-110)^*$-plane of the Pt matrix (Figure 1(i)) is coincident with the $(-110)^*$ plane of a fcc bulk crystal shown by the inset in Figure 3(a). In principal, the stacking fault (abab-growth instead of abcabc-growth for fcc growth) could occur during the epitaxial growth, but no streaked spots due to the stacking fault perpendicular to the sample surface were observed by RHEED shown in Figure 1(f); therefore the epitaxial growth with the hcp-stacking fault could be excluded. However, no extra reflection spots appear at $[0110]_{Ru}$ azimuth in the RHEED pattern (Figure 1(g)); the interpretation for that and the origin of the extra spots appeared at [11-20] azimuth in Figure 1(f) will be elucidated in Section 4 (discussion).

3.2. Spontaneous and Electrodeposition of Ru on Pt(111). The LEED and RHEED patterns (Figures 4(a) and 4(b)) for Pt(111) covered with Ru (~0.27 ML) by spontaneous deposition show a (1×1) structure, which is entirely similar to that obtained for a clean Pt(111) surface (not shown, refer to [7]). But a pronounced Auger Ru-signal develops at 275 eV in Figure 5(b) (compare with that of a clean surface 5(a)), confirming the presence of Ru deposit on Pt(111). Moreover, there is no intensity modulation along the streaked substrate reflections in RHEED, differing from that found for Pt on Ru(0001) (compare with Figures 1(c) and 1(d)), implying that the Ru deposit forms monolayer islands on Pt(111), in good agreement with that found by the in situ STM investigations [25], in which the average diameter of the two-dimensional Ru islands is in the range of 1–3 nm, where the Ru spontaneous deposition was performed by the Pt(111) electrode immersion in 1 mM $RuCl_3$ + 0.1 M $HClO_4$ solution for 3 minutes. Similar results have been found by Crown et al. [38, 39]; they found that the Ru islands appear very uniformly distributed across the surface, with an islands diameter ranging from 2 to 5 nm for Ru deposition on Pt(111) immersed in 0.5 mM $RuCl_3$ + 0.1 M $HClO_4$ solution for 20 seconds. The islands seem to nucleate without preference of terrace or steps. The thickness of Ru layers increases with the immersion time [40]. Since the 2D reflection rods of Ru coincide with the Pt substrate (±10) rods in RHEED, the [11-20] atomic row spacing of Ru matches to the [−110] atomic row spacing of the Pt(111) substrate. Thus the Ru deposit grows a (1×1) commensurate layer with +2.5% expansion with respect to the bulk Ru on Pt(111). The 2D-islands are scattered in phase; it is therefore difficult to obtain the size-distribution of the Ru islands by RHEED [41]. However, the increased charge in the double-layer region of the cyclic voltammogram may indicate that the monolayer thick Ru islands cover about 20% of the Pt(111) substrate surface [7]. At 0.64 coverage the intensity modulation develops along the Pt substrate reflections (Figures 4(c) and 4(d)); Ru bilayer thick island growth is found by analysis of the intensity-profile of the substrate reflection rods [7]. Some population of third and higher layers may also be present on Pt(111) as observed by STM [25, 40]. An average domain size of about 4.4 nm has been estimated from the spot width of the RHEED pattern shown in Figure 4(d), and the height of the clusters

is about 0.5 nm from the spot width in c-direction close to two-layer height. Moreover, additional satellite reflections depicted by arrows develop outside of the ($\pm$10) and ($\pm$11) substrate reflections in RHEED (Figures 4(c) and 4(d)). In order to determine precisely the spacing of satellite and of Pt substrate reflections, we measure the spot spacing of the Pt substrate denoted by arrows at the first Laue-zone in Figure 4(e) and the satellite reflection spacing of Ru in the zero Laue-zone (2D surface reflections) (refer to Figure 4(e)). It is found that the spacing of satellite reflections is $\cong$3% larger than that of the Pt substrate, indicating that Ru adlayer relaxes to its bulk lattice constant, consistent with the detected spot spacing of 0.458 A^{-1} along the (00) rod in Figure 4(d), that is the (002)-reciprocal lattice spacing of the bulk Ru(0001) (0.467 A^{-1}). These data reflect the fact that the Ru deposit forms an incommensurate adlayer on Pt(111). At higher coverage ($\sim$1 ML) the Ru islands thicken rapidly, leading to 3D cluster formation shown by RHEED (Figures 4(f) and 4(g)), having an average cluster size of $\sim$2 nm (estimated from the spot width). The spot spacing along the (00) reflection rod is also 0.458 A^{-1} (Figure 4(g)), equal to that observed for the bilayer island growth; that is, both 2D-island and 3D-clusters of Ru are growing with (0001) plane parallel to Pt(111). The corresponding AES spectrum in Figure 5(c) shows that the Auger Ru-signal increases significantly, in line with the RHEED observations (Figures 4(f) and 4(g)), whereby the pronounced Ru reflections develop. On the other hand, the Ru deposited on Pt(111) prepared by Ru vapor deposition in UHV shows 3D-islands having a width of 5–10 nm and multilayer thick by STM [27]. The difference in the size distribution of the clusters from that obtained by electrodeposition ($\sim$2 nm) is apparently due to the evaporation rate of Ru in UHV and the subsequent annealing at 800 K. The subsequent annealing to 800 K leads to these islands to collapse and induces a ripening process, resulting in large, multilayer islands [27]. We are questioning whether the 3D-spots in the RHEED (Figure 4(f)) are due to the Pt or Ru nanoclusters. It is rather difficult to distinguish the Pt clusters from that of Ru or Pt-Ru alloys grown on Pt(111) by STM. For RHEED the answer lies in a comparison of the rel-plane $(-110)^*$ of a fcc bulk Pt (refer to the inset in Figures 3(a) and 1(f)) with that of a hcp bulk Ru. Because at [$-$211] azimuth (Figure 4(g)), the reflection spots are quite diffuse and broad, and the Pt (02-2)-spot spacing (0.72 A^{-1}) with respect to the (00) rod, which is just below the 1–13 spot (refer to Figure 1(h)), is only $\sim$ 1% smaller than that of the Ru (1-20)-spot (0.738 A^{-1}) (see Figure 4(g)), it is rather difficult to distinguish the Pt- from Ru-spot at this azimuth. However, at [$-$110] azimuth the (1-13) and ($-$113) spots in the $(110)^*$-plane of bulk Ru have the same rel-distances coincident with those observed in Figure 4(f), since the sum of the squares of their indices are the same, while the rel-distance of the 220- and 113-spots of fcc bulk Pt in the $(-110)^*$-plane are unequal (refer to the inset in Figure 3(a)). From the comparison we conclude that the observed RHEED pattern in Figure 4(f) is a $(110)^*$-plane of hcp bulk Ru, so that the reflection spots in Figure 4(f) are due to the Ru-nanoclusters rather than Pt-clusters or Pt-Ru alloy grown on Pt(111). And the close packed [11-20] direction of the Ru deposit is parallel to the close packed [$-$110] direction of the Pt (111) substrate.

4. Discussion

At $\sim$0.4 coverage pseudomorphic bilayer Pt islands were preferably formed on Ru(0001), in which the lateral spacing of the Pt layers was compressed by $\sim$2.5% with respect to bulk Pt due to the mismatch of Pt and Ru. After the second spontaneous deposition, twinning developed in the 2-3 layer thick islands while the lattice strain induced by pseudomorphic growth is fully present, since the Pt twin spots coincide with the Ru substrate reflection streaks indicating that the lateral spacing of the Pt clusters matches to that of the Ru substrate. After identification of the well-defined extra spots with respect to the Pt matrix spots in Figure 1(j) by the twinning matrix as demonstrated below, we are able to assign the extra spots depicted by arrow in Figure 1(e) to twinning with the aid of Figure 1(k). Hence we are able to detect the initial stage of the twin formation in 2-3 layer thick Pt film on Ru(0001) (Figures 1(c) and 1(e)). At higher coverage ($\sim$10 ML thickness) Pt relaxes to its bulk lattice constant (3.92 A) in agreement with that observed in UHV, for that the dislocation lines were observed in the STM images for 8 ML Pt on Ru(0001), while the dislocation lines were absent at 4 ML coverage [22]. The lattice strain relief by increased layer thickness has also been observed for Co on Pt(111) [28], Cu on Ru(0001) [30], and Pd on Au(100) [6]; for instance at low coverage the lateral spacing of the Pd layers is compressed with respect to bulk Pd to match with the Au(100) substrate, but at higher coverage the Pd lattice relaxes to that of the bulk Pd. We are questioning whether the additional 3D-spots in the RHEED (Figures 1(f) and 1(i)) are due to the Pt-clusters with a hcp phase grown on Ru(0001). If the hcp Pt-clusters were present, they would favored grow in (0001) orientation with respect to the Pt(111) surface to minimize the surface strain as the (0001) Ru clusters grow on Pt(111). As a consequence, the rel-spacing of a hcp (002) spot (0.51 A^{-1}) of the Pt clusters would be about 15% larger than that of (111) (0.442 A^{-1}) of a fcc phase (spacing of the 111-matrix spot), and the location of the hcp reflection spots with respect to the matrix spots would be not regularly positioned, one third of the Pt matrix spots along the $\langle 111 \rangle$ directions as that observed in Figures 1(f) and 1(i). Moreover, some of the hcp spots would develop in the region between the (00) and the ($\pm$10) substrate reflection rods, being contradictory to the observed pattern in Figure 1(i). The coexistence of hcp and fcc clusters grown on Ru(0001) can thus be excluded in the present Pt/Ru(0001) system. As expected the Pt (111) cluster adopts favored the fcc bulk phase grown on Ru(0001) to minimize the surface strains. It is worthy to mention that the intermixing of Pt and Ru is difficult to detect by STM [21, 23, 27], since a clear assignment of a certain brightness in the STM image to either Pt or Ru is difficult, especially as the contrast found depends strongly on the status of the tunneling tip [21, 42, 43]. On the other hand, if the Pt-Ru alloy were formed after the Pt deposition on

Ru(0001), the additional reflections due to the alloy would appear in the RHEED patterns, like that known for the Hg-Pt alloy formation on Pt(111) by Hg electrodeposition at room temperature [44]. For that the estimated lattice constants of $PtHg_2$ and $PtHg_4$ alloys by RHEED agree nicely with those of X-ray measurements. Since no additional reflections of the Pt-Ru alloy were observed by RHEED, we conclude that the intermixing of Pt and Ru is absent at room temperature in the Pt/Ru(0001) systems.

Now let us index the extra spots developed in the RHEED patterns, for example, Figure 1(i), in which they are regularly positioned, one third of the Pt matrix spots along the ⟨111⟩ directions, indicative of the presence of twinning. We will demonstrate that the reciprocal lattice of the extra spots will be related to that of the original crystal by the twinning matrix [45, 46] as follows:

$$(\mathrm{PQR})_T = T_{hkl} \cdot (\mathrm{pqr})_M = \frac{1}{3}\begin{pmatrix} -1 & 2hk & 2hl \\ 2hk & -1 & 2kl \\ 2hl & 2kl & -1 \end{pmatrix} \cdot (\mathrm{pqr})_M, \tag{1}$$

where T_{hkl} is the twinning matrix, and $(\mathrm{PQR})_T$ and $(\mathrm{pqr})_M$ are the relps of the twin and the matrix, respectively. The extra spots appear along the ⟨111⟩ directions (see Figure 1(i)); hence there is twinning about the ⟨111⟩ axis normal to the face. The operator T_{111} transforms $(002)_M$ into $1/3\cdot(44\text{-}2)_T$ and $(220)_M$ into $1/3\cdot(228)_T$ (refer to Figure 1(k)). The $1/3(44\text{-}2)_T$ twin spot can be expressed by vector addition, $(11\text{-}1)_M + 1/3(111)$, which means that the twin spot is displaced from the $(11\text{-}1)_M$ matrix point by the vector $+1/3\langle 111\rangle$ along the (10) beam (refer to Figure 1(k)), in agreement with the observed RHEED pattern in Figure 1(j). The same holds for the twin spot $1/3(228)_T$ (refer to Figure 1(k)), which is displaced from the $(113)_M$ point by $-1/3\langle 111\rangle$ along the (-10)-beam. However, at the $[-211]_{\mathrm{Pt}}$, [0110] azimuth, the twin point $(1\text{-}13)_T$ (see Figure 1(h)), obtained from the matrix point $(13\text{-}1)_M$ ($T_{111}\cdot (13\text{-}1)_M = (1\text{-}13)_T$) at the (11)-beam, coincides exactly with the matrix point $(1\text{-}13)_M$ at the $(-1\text{-}1)$ beam (refer to Figure 1(h)), since the sum of the squares of their indices are the same and the Bragg angles are also the same. The same holds for other twin points at this azimuth; hence no extra spots are visible at this azimuth in Figure 1(g). For clarity the reciprocal lattice of the Pt parent matrix in Figure 1(j) is sketched in Figure 3(b). Since the lattice orientation of the twins differs from that of the parent matrix, they will give their own set of reflection spots as shown by Figure 3(c), which is obtained by the twinning transformation of Figure 3(b). Consequently, the RHEED pattern in Figure 1(i) is a result of the superposition of the reciprocal lattices of the matrix and the twin. The additional reflection spots denoted by D_1 and D_2 between the 111 and 222 reflections at the [11-20] azimuth (refer to Figure 1(k)) are due to double diffractions between the two crystals (matrix and twin), which are illustrated with the aid of the inset in Figure 1(k) by vector-addition:

$$\begin{aligned} D_1 &= g_{002}(\text{matrix}) + \frac{1}{3}T_{111}(002)_M \\ &= \vec{g}_{002}(\text{matrix}) + \frac{1}{3}\cdot(44-2)_T \\ &= \frac{1}{3}(444) = (111)_M + \frac{1}{3}(111). \end{aligned} \tag{2}$$

Thus the RHEED patterns are completely indexed and the extra spots are neither due to the stacking fault of the Ru substrate nor the Pt-Ru alloys as observed for PtHg-alloy formed by Hg electrodeposition on Pt(111) [44], but rather are due to twinning. Note that the rel-plane $(-110)^*$ of the matrix (Figure 3(b)) coincides with that of the twin (Figure 3(c)) by reflection about the (11-2) mirror plane. It becomes evident that twins are formed by two orientations nucleated side by side separated by an incoherent twin boundary (11-2), illustrated by Figure 3(d), in which the Pt deposit grown on the basal plane of Ru(0001) forms two orientations, one orientation is stacked abA-bcabc... and the other is abA-cbacb..., where A represents the atom position in the Ru substrate surface (refer to Figure 3(d)).

For the Ru deposit on Pt(111), at low Ru coverage (∼0.3), a (1×1) commensurate layer with monolayer thick islands was observed nicely in agreement with the in situ STM investigations, in which most of the islands (76%) have monolayer height at 0.2 ML coverage, but a detectable amount of the multilayer growth appears as well on Pt(111) [25]. Due to the coincidence of the Pt- and Ru-rods in RHEED, it is found that Ru adlayer is expanded by +2.5% with respect to the bulk Ru to match with the Pt(111) surface. At coverage ∼0.64, bilayer thick islands develop consistent with STM investigations [25], where Ru islands are predominantly formed on top of the previously adsorbed islands. The remarkable behavior of 2D islands growth has also been observed for Cu vapor-deposition onto ZnO at room temperature and below [47]. Moreover, it is found that adsorption of the second Ru layer leads to relief of the strain in the first layer, giving rise to dislocations and incommensurate bilayer islands demonstrated by the satellite reflections; a similar behavior has also been found for Ag on Pt(111) [29]. Higher Ru coverage >1 ML results in cluster formation (see Figures 4(f) and 4(g)); thereby the Ru relaxes to its bulk lattice constant, confirmed also by the detected spot spacing of the (002) reflection along the (00) rod, corresponding to the bulk Ru. Although the intensity of the (-112) spot, which is located between the -113 and -111 spots, is around one fourth that of the (-111) spot (see Figure 4(f)), it is not resolved and smeared, indicating that the stacking fault is obviously present in the Ru deposit, supported also by the streaked (-122) spot in Figure 4(g). Both 2D islands and 3D clusters of Ru grow in the (0001) orientation on Pt(111).

It is informative to compare our results with related experiments. The spontaneous deposition of Pt on Ru(0001) has been recently studied using the XPS technique [24], in which the PtO species are mainly observed on Ru(0001) based on the XPS data analyses, whilst amorphous Pt

oxide surface layers have been observed by X-ray study for a Pt/SiO_2 sample oxidized under 1 bar at 300°C [48]. If both amorphous Pt oxide and the Pt(II)O oxide with a cubic phase [49] or a tetragonal phase [50] were present, additional reflections due to the Pt oxide would appear in the RHEED, whereas only the reflections of the crystalline Pt-clusters were observed by RHEED in agreement with the in situ STM investigations [5], where the entire Ru(0001) surface was covered with 2–6 nm sized Pt crystallites after Pt spontaneous deposition on Ru(0001). Up to $n = \sim 3$–5 ML Pt grows pseudomorphically on Ru(0001) prepared by electrodeposition nicely in agreement with the recently reported work for Pt deposited on Ru(0001) under UHV conditions [22, 23]; they find that the lattice strain still remains on Ru(0001) up to at least $n = 4$ ML, and a rapid increase of the CO bond strength and a reduction in CO desorption energy is observed on the strained Pt layers [22, 23]. This finding is in line with our previous results [16], in which the strained Pt adlayer on the Ru(10-10) surface leads to lowering of the CO oxidation potential and, as a consequence, to an enhanced CO electrooxidation [51]. Similarly, a distinct lower desorption/oxidation energy of CO on Pt/Ru(0001) with respect to pure Pt and Ru(0001) has also been observed under UHV conditions [21], in which the reduction in CO adsorption energy is attributed to the electronic modification of the Pt deposit with Ru(0001). Although numerous microtwins forming on the evaporated fcc metal films on sodium chloride have been observed by transmission electron microscopy [52], while twins growing on massive metal substrates are seldom reported due to the limitation of sample preparations. As far as we know, there were no reports about the twin formation for Pt deposit on Ru(0001) prepared in both electrochemical [4, 5, 24] and UHV environments [21–23]. Several mechanisms for the twin formation in evaporated films have been proposed. Burbank and Heidenreich suggested that twins were formed to accommodate the displacement between the lattices of coalescing nuclei [52], while Matthews and Allinson [53] proposed that twins are formed when two nuclei, which happen to be approximately twins of one another, coalesce and rotate into a precisely twin relationship. Perhaps the best known of these is due to Menzer [54] and Pashley [55]; they suggested that silver grew initially in the twin orientations and that the final orientation of the nanoclusters results from twinning of the initial ones. We find that Pt twinning occurs in 2-3 ML thick islands on Ru(0001) which is close to that found for Au deposits on NaCl [53], as they found that Au twin coalescence occurred in 10 A (~4 ML), but more commonly in 20 A specimens. And we claim that twin nuclei develop initially in Pt deposited film and they are epitaxially growing up from twinning of the initial ones, since the epitaxial growth of twinned Pt nanoparticles on Ru(0001) is independent of the nucleation kinetics. The growth features of twinned Pt particles on Ru(0001) are significant because they have not been reported so far in an electrochemical environment. Interestingly, in the inverse system, no twinning occurs in the Ru deposit on Pt(111), while a stacking fault in thicker Ru islands has been observed. Moreover, twinned Pt clusters were absent in evaporated Pt films on γ-Al_2O_3 oxide surface [56] and oxide film grown on NiAl(100) [55] under UHV conditions, where randomly oriented Pt clusters developed at 300 K as shown by the Debye-Scherre rings in RHEED [57]. It is likely that the random orientation of the Pt particles is due to the weak interaction between clusters and oxide substrate surfaces. Nevertheless, the Pt [57] and Co [58] clusters grow with the (001) facets parallel to the (001) oxide film grown on NiAl(100), while the Pt clusters grow with the (111) facet on the γ-Al_2O_3 oxide surface [56] in order to reduce the lattice mismatch. Similar trends have also been found for the Pt and Ru clusters growing with the facets of hexagonal unit mesh on the Ru(0001) and Pt(111) substrates, respectively.

5. Conclusion

Pt grows pseudomorphically on Ru(0001) up to at least 4 ML, for which the lattice strain within the film still remains and is completely released after cluster formation on Ru(0001). We report here for the first time observing that the initial stage of twin formation occurs in 2-3 ML thick Pt islands on Ru(0001) in an electrochemical environment. There is twinning about the ⟨111⟩ axis normal to the substrate surface, and the parent matrix and twin are separated by the (11-2) twin plane normal to Ru(0001), and no multiple twinning is observed at any Pt coverage. It seems that the twin nuclei develop initially in Pt deposited film, and with increasing coverage they are epitaxially growing up from twinning of the initial ones, since the epitaxial growth of twinned Pt nanoparticles on Ru(0001) is independent of nucleation kinetics, that is, deposition processes (spontaneous/electrodeposition). Furthermore, the coexistence of the hcp and fcc clusters grown on Ru(0001) can be excluded in the Pt/Ru(0001) system, since the reflection spots of the hcp clusters would not be positioned, one third of the matrix spots along the ⟨111⟩ direction as that observed by RHEED. Also the intermixing of Pt and Ru is excluded, since the additional reflections of the Pt-Ru alloy are absent in RHEED.

For an Ru deposit on Pt(111), at low coverage (~0.2), monolayer thick islands with 2.5% lateral expansion with respect to the bulk Ru are formed on Pt(111). Up to ~0.64 coverage, the second layer is found to relieve the strain in the first layer, giving rise to the incommensurate bilayer (0001) islands on Pt(111). Whilst the Pt lattice strain releases at multilayer islands (>3 monolayers) on Ru(0001), yet, the origin of the difference in layer dependence of the lattice strain for Pt and Ru is not known. At coverages higher than 1 ML, the (0001) Ru clusters are formed and aligned with their [11-20] direction parallel to the [−110] substrate direction, whereby the hcp stacking fault in the Ru deposit apparently occurs on Pt(111).

References

[1] T. Iwasita, H. Hoster, A. John-Anacker, W. F. Lin, and W. Vielstich, "Methanol oxidation on PtRu electrodes. Influence of surface structure and Pt-Ru atom distribution," *Langmuir*, vol. 16, no. 2, pp. 522–529, 2000.

[2] J. C. Davies, B. E. Hayden, and D. J. Pegg, "The electrooxidation of carbon monoxide on ruthenium modified Pt(110)," *Electrochimica Acta*, vol. 44, no. 6-7, pp. 1181–1190, 1998.

[3] E. Herrero, K. Franaszczuk, and A. Wiecskowski, "A voltammetric identification of the surface redox couple effective in methanol oxidation on a ruthenium-covered platinum (110) electrode," *Journal of Electroanalytical Chemistry*, vol. 361, no. 1-2, pp. 269–273, 1993.

[4] M. S. Zei, T. Lei, and G. Ertl, "Spontaneous and electrodeposition of Pt on Ru(0001)," *Zeitschrift für Physikalische Chemie*, vol. 217, no. 5, pp. 447–458, 2003.

[5] S. R. Brankovic, J. McBreen, and R. R. Adžić, "Spontaneous deposition of Pt on the Ru(0001) surface," *Journal of Electroanalytical Chemistry*, vol. 503, no. 1-2, pp. 99–104, 2001.

[6] A. L. N. Pinheiro, M. S. Zei, M. F. Luo, and G. Ertl, "The epitaxial growth of Pd electrodeposition on Au(1 0 0) studied by LEED and RHEED," *Surface Science*, vol. 600, no. 3, pp. 641–650, 2006.

[7] W. F. Lin, M. S. Zei, M. Eiswirth, G. Ertl, T. Iwasita, and W. Vielstich, "Electrocatalytic activity of Ru-modified Pt(111) electrodes toward CO oxidation," *Journal of Physical Chemistry B*, vol. 103, no. 33, pp. 6968–6977, 1999.

[8] S. Strbac, O. M. Magnussen, and R. J. Behm, "Nanoscale pattern formation during electrodeposition: Ru on reconstructed Au(111)," *Physical Review Letters*, vol. 83, no. 16, pp. 3246–3249, 1999.

[9] Z. Jusys, J. Kaiser, and R. J Behm, "Composition and activity of high surface area PtRu catalysts towards adsorbed CO and methanol electrooxidation—a DEMS study," *Electrochimica Acta*, vol. 47, no. 22-23, pp. 3693–3706, 2002.

[10] E. A. Batista, H. Hoster, and T. Iwasita, "Analysis of FTIRS data and thermal effects during methanol oxidation on UHV-cleaned PtRu alloys," *Journal of Electroanalytical Chemistry*, vol. 554-555, no. 1, pp. 265–271, 2003.

[11] A. A. El-Shafei, R. Hoyer, L. A. Kibler, and D. M. Kolb, "Methanol oxidation on Ru-modified preferentially oriented Pt electrodes in acidic medium," *Journal of the Electrochemical Society*, vol. 151, no. 6, pp. F141–F145, 2004.

[12] B. E. Hayden, M. E. Rendall, and O. South, "Electro-oxidation of carbon monoxide on well-ordered Pt(111)/Sn surface alloys," *Journal of the American Chemical Society*, vol. 125, no. 25, pp. 7738–7742, 2003.

[13] E. I. Santiago, G. A. Camara, and E. A. Ticianelli, "CO tolerance on PtMo/C electrocatalysts prepared by the formic acid method," *Electrochimica Acta*, vol. 48, no. 23, pp. 3527–3534, 2003.

[14] E. I. Santiago, M. J. Giz, and E. A. Ticianelli, "Studies of carbon monoxide oxidation on carbon-supported platinum-osmium electrocatalysts," *Journal of Solid State Electrochemistry*, vol. 7, no. 9, pp. 607–613, 2003.

[15] H. A. Gasteiger, N. M. Marković, and P. N. Ross Jr., "H_2 and CO electrooxidation on well-characterized Pt, Ru, and Pt-Ru. 1. Rotating disk electrode studies of the pure gases including temperature effects," *Journal of Physical Chemistry*, vol. 99, no. 20, pp. 8290–8301, 1995.

[16] A. L. N. Pinheiro, M. S. Zei, and G. Ertl, "Electro-oxidation of carbon monoxide and methanol on bare and Pt-modified Ru(1010) electrodes," *Physical Chemistry Chemical Physics*, vol. 7, no. 6, pp. 1300–1309, 2005.

[17] R. Ianniello, V. M. Schmidt, U. Stimming, J. Stumper, and A. Wallau, "CO adsorption and oxidation on Pt and PtRu alloys: dependence on substrate composition," *Electrochimica Acta*, vol. 39, no. 11-12, pp. 1863–1869, 1994.

[18] W. Chrzanowski, H. Kim, and A. Wieckowski, "Enhancement in methanol oxidation by spontaneously deposited ruthenium on low-index platinum electrodes," *Catalysis Letters*, vol. 50, no. 3-4, pp. 69–75, 1998.

[19] K. A. Friedrich, K.-P. Geyzers, A. Marmann, U. Stimming, and R. Vogel, "Bulk metal electrodeposition in the sub-monolayer regime: Ru on Pt(111)," *Zeitschrift für Physikalische Chemie*, vol. 208, no. 1-2, pp. 137–150, 1999.

[20] W. Chrzanowski and A. Wieckowski, "Ultrathin films of ruthenium on low index platinum single crystal surfaces: an electrochemical study," *Langmuir*, vol. 13, no. 22, pp. 5974–5978, 1997.

[21] F. Buatier, B. De Mongeot, M. Scherer, B. Gleich, E. Kopatzki, and R. J. Behm, "CO adsorption and oxidation on bimetallic Pt/Ru(0001) surfaces—a combined STM and TPD/TPR study," *Surface Science*, vol. 411, no. 3, pp. 249–262, 1998.

[22] A. Schlapka, M. Lischka, A. Groß, U. Käsberger, and P. Jakob, "Surface strain versus substrate interaction in heteroepitaxial metal layers: Pt on Ru(0001)," *Physical Review Letters*, vol. 91, no. 1, Article ID 016101, 4 pages, 2003.

[23] P. Jakob and A. Schlapka, "CO adsorption on epitaxially grown Pt layers on Ru(0 0 0 1)," *Surface Science*, vol. 601, no. 17, pp. 3556–3568, 2007.

[24] S. Manandhar and J. A. Kelber, "Spontaneous deposition of Pt and Ir on Ru: reduction to intermediate oxidation states," *Electrochimica Acta*, vol. 52, no. 15, pp. 5010–5017, 2007.

[25] S. Strbac, C. M. Johnston, G. Q. Lu, A. Crown, and A. Wieckowski, "In situ STM study of nanosized Ru and Os islands spontaneously deposited on Pt(111) and Au(111) electrodes," *Surface Science*, vol. 573, no. 1, pp. 80–99, 2004.

[26] S. Cramm, K. A. Friedrich, K.-P. Geyzers, U. Stimming, R. Vogel, and J. Fresenius, "Surface structural and chemical characterization of Pt/Ru composite electrodes: a combined study by XPS, STM and IR spectroscopy," *Fresenius' Journal of Analytical Chemistry*, vol. 358, no. 1-2, pp. 189–192, 1997.

[27] H. Hoster, T. Iwasita, H. Baumgärtner, and W. Vielstich, "Pt-Ru model catalysts for anodic methanol oxidation: influence of structure and composition on the reactivity," *Physical Chemistry Chemical Physics*, vol. 3, no. 3, pp. 337–346, 2001.

[28] E. Lundgren, B. Stanka, M. Schmid, and P. Varga, "Thin films of Co on Pt(111): strain relaxation and growth," *Physical Review B*, vol. 62, no. 4, pp. 2843–2851, 2000.

[29] H. Brune, H. Röder, C. Boragno, and K. Kern, "Strain relief at hexagonal-close-packed interfaces," *Physical Review B*, vol. 49, no. 4, pp. 2997–3000, 1994.

[30] G. O. Potschke and R. J. Behm, "Interface structure and misfit dislocations in thin Cu films on Ru(0001)," *Physical Review B*, vol. 44, no. 3, pp. 1442–1445, 1991.

[31] G. Lehmpfuhl, Y. Uchida, M. S. Zei, and D. M. Kolb, "Electron diffraction and electron microscopy of electrode surfaces," in *Imaging of Surfaces and Interfaces; Frontiers of Electrochemistry*, J. Lipkowski and P. N. Ross, Eds., vol. 5, p. 57, Wiley-VCH, Weinheim, Germany, 1999.

[32] W. Lin, M. S. Zei, Y. D. Kim, H. Over, and G. Ertl, "Electrochemical versus gas-phase oxidation of ru single-crystal surfaces," *Journal of Physical Chemistry B*, vol. 104, no. 25, pp. 6040–6048, 2000.

[33] M. Watanabe and S. Motoo, "Electrocatalysis by ad-atoms part II. Enhancement of the oxidation of methanol on platinum by ruthenium ad-atoms," *Journal of Electroanalytical Chemistry*, vol. 60, no. 3, pp. 267–273, 1975.

[34] L. E. Davis, N. C. Mac Donald, P. W. Palmberg, G. E. Riach, and R. F. Weber, *Handbook of Auger Electron Spectroscopy*, Physical Electronics Industries, Eden Prairie, MN, USA, 1976.

[35] W. B. Wang, M. S. Zei, and G. Ertl, "Electrosorption and electrooxidation of CO on Ru(0001)," *Physical Chemistry Chemical Physics*, vol. 3, no. 16, pp. 3307–3311, 2001.

[36] G. Ertl and J. Kueppers, *Low Energy Electron Diffraction and Surface Chemistry*, VCH, Weinheim, Germany, 1985.

[37] P. Gassmann, R. Franchy, and H. Ibach, "Investigations on phase transitions within thin Al_2O_3 layers on NiAl(001)—HREELS on aluminum oxide films," *Surface Science*, vol. 319, no. 1-2, pp. 95–109, 1994.

[38] M. S. Zei, G. Qiao, G. Lehmpfuhl, and D. M. Kolb, "Influence of anions on the structure of underpotentially deposited Cu on Au(111): a LEED, RHEED, and AES study," *Berichte der Bunsen-Gesellschaft für Physikalische Chemie*, vol. 91, no. 4, pp. 349–353, 1986.

[39] N. Batina, T. Will, and D. M. Kolb, "Study of the initial stages of copper deposition by in situ scanning tunnelling microscopy," *Faraday Discussions*, vol. 94, pp. 93–106, 1992.

[40] A. Crown, I. R. Moraes, and A. Wieckowski, "Examination of Pt(111)/Ru and Pt(111)/Os surfaces: STM imaging and methanol oxidation activity," *Journal of Electroanalytical Chemistry*, vol. 500, no. 1-2, pp. 333–343, 2001.

[41] R. L. Park, "LEED studies of surface imperfections," in *The Structure and Chemistry of Solid Surfaces*, G. A. Somorjai, Ed., p. 28, John Wiley & Sons, New York, NY, USA, 1969.

[42] J. A. Rodriguez, "Physical and chemical properties of bimetallic surfaces," *Surface Science Reports*, vol. 24, no. 7-8, pp. 223–287, 1996.

[43] M. Scherer, Diplom Thesis, Universitaet Konstanz/Universitaet Ulm, 1997.

[44] H. L. Wu, S. Yau, and M. S. Zei, "Crystalline alloys produced by mercury electrodeposition on Pt(1 1 1) electrode at room temperature," *Electrochimica Acta*, vol. 53, no. 20, pp. 5961–5967, 2008.

[45] D. W. Pashley and M. J. Stowell, "Electron microscopy and diffraction of twinned structures in evaporated films of gold," *Philosophical Magazine*, vol. 8, no. 94, pp. 1605–1632, 1963.

[46] O. Johari and G. Thoma, *Stereographic Projection and Applications*, Wiley-Interscience, New York, NY, USA, 1969.

[47] K. H. Ernst, A. Ludviksson, R. Zhang, J. Yoshihara, and C. T. Campbell, "Growth model for metal films on oxide surfaces: Cu on ZnO(0001)-O," *Physical Review B*, vol. 47, no. 20, pp. 13782–13796, 1993.

[48] V. Gnutzmann and W. Vogel, "Structural sensitivity of the standard Pt/SiO2 catalyst EuroPt-1 to H_2 and O_2 exposure by in situ X-ray diffraction," *Journal of Physical Chemistry*, vol. 94, no. 12, pp. 4991–4997, 1990.

[49] J. Kumar and R. Saxena, "Formation of NaCl- and Cu_2O-type oxides of platinum and palladium on carbon and alumina support films," *Journal of the Less-Common Metals*, vol. 147, no. 1, pp. 59–71, 1989.

[50] W. J. Moore Jr. and L. Pauling, "The crystal structures of the tetragonal monoxides of lead, tin, palladium, and platinum," *Journal of the American Chemical Society*, vol. 63, no. 5, pp. 1392–1394, 1941.

[51] P. N. Ross, K. Kinoshita, A. J. Scarpellino, and P. Stonehart, "Electrocatalysis on binary alloys II. Oxidation of molecular hydrogen on supported Pt+Ru alloys," *Journal of Electroanalytical Chemistry*, vol. 63, no. 1, pp. 97–110, 1975.

[52] R. D. Burbank and R. D. Heidenreich, "Microtwinning in epitaxial nickel-iron films," *Philosophical Magazine*, vol. 5, no. 52, pp. 373–382, 1960.

[53] J. W. Matthews and D. L. Allinson, "A mechanism for the formation of twins in evaporated face-centred cubic metal films," *Philosophical Magazine*, vol. 8, no. 92, pp. 1283–1303, 1963.

[54] G. Menzer, "Zwillingsnetze und regelmaessige Verwachungen der dichtesten Kugelpackungen," *Zeitschrift für Kristallographie*, vol. 99, pp. 378–409, 1938.

[55] D. W. Pashley, "The study of epitaxy in thin surface films," *Advances in Physics*, vol. 5, no. 18, pp. 173–240, 1956.

[56] J. Libuda, M. Bäumer, and H. J. Freund, "Structural characterization of platinum deposits supported on ordered alumina films," *Journal of Vacuum Science & Technology A*, vol. 12, no. 4, pp. 2259–2264, 1994.

[57] M. F. Luo, W. H. Wen, C. S. Lin, C. I. Chiang, S. D. Sartale, and M. S. Zei, "Structures of Co and Pt nanoclusters on a thin film of Al_2O_3/NiAl(1 0 0) from reflection high-energy electron diffraction and scanning-tunnelling microscopy," *Surface Science*, vol. 601, no. 10, pp. 2139–2146, 2007.

[58] M. S. Zei, "Epitaxial growth of cobalt clusters on the bare and the oxide film grown on NiAl(1 0 0) surfaces," *Surface Science*, vol. 601, no. 3, pp. 858–864, 2007.